Research Paper

GEOSPHERE

GEOSPHERE, v. 15, no. 6

https://doi.org/10.1130/GES02164.1

5 figures; 4 tables; 1 supplemental file

CORRESPONDENCE: p.j.mcphee@uu.nl; peter.mcphee@live.co.uk

CITATION: McPhee, P.J., van Hinsbergen, D.J.J., and Thomson, S.N., 2019, Thermal history of the western Central Taurides fold-thrust belt: Implications for Cenozoic vertical motions of southern Central Anatolia: Geosphere, v. 15, no. 6, p. 1927–1942, https://doi.org/10.1130/GES02164.1.

Science Editor: Shanaka de Silva
Associate Editor: Michael L. Williams

Received 13 May 2019
Accepted 19 August 2019

Published online 7 November 2019

Thermal history of the western Central Taurides fold-thrust belt: Implications for Cenozoic vertical motions of southern Central Anatolia

Peter J. McPhee[1], Douwe J.J. van Hinsbergen[1], and Stuart N. Thomson[2]

[1]Department of Earth Sciences, Utrecht University, Princetonlaan 8A, 3584 CB Utrecht, the Netherlands
[2]Department of Geosciences, University of Arizona, Tucson, Arizona 85721, USA

ABSTRACT

The modern physiography of central Turkey is dominated by the 1-km-high Central Anatolian Plateau and the Central Tauride mountains that form the southern plateau margin. These correspond to a Cretaceous–Eocene backarc extensional province and forearc fold-thrust belt, respectively. The extent to which the morphology of the Miocene plateau was inherited from the physiography of the Cretaceous–Eocene subduction zone that assembled the Anatolian crust has not been tested but is important if we are to isolate the signal of Miocene and younger subduction dynamics in the formation of the modern plateau margin. There is no known stratigraphic record of the post-Eocene pre-Miocene evolution of the Taurides. We therefore collected rock samples across the Taurides and used zircon (U-Th)/He (ZHe), apatite (U-Th)/He (AHe), and apatite fission-track (AFT) low-temperature thermochronometers to constrain cooling; we interpret these thermochronometers to signal erosional exhumation. We use inverse thermal modeling to aid interpretation of our results and find that: (1) thermochronometers across the Taurides were reset as a result of heating by the emplacement of the Antalya and Bozkır nappes; (2) AFT and ZHe Eocene cooling ages are related to structurally driven uplift and erosional exhumation on major thrust culminations; (3) dispersed AHe ages record low rates of Oligocene–early Miocene cooling and hence low rates of erosional exhumation; and (4) fast rates of cooling were determined for samples along the margin of the Köprüçay Basin. We interpret that early Miocene cooling is a signal of active erosion of the western Central Taurides at a time of marine sedimentation in the Mut Basin on the southern Central Taurides, and these differing histories may reflect evolution above the Antalya and Cyprus slabs. Our thermochronological data, the enigmatic development of the Antalya Basin, and thrusting within the basin may be explained as the surface expression of stepwise delamination of the Antalya slab from the Tauride hinterland to its current position below the Gulf of Antalya since early Miocene time over a distance of ~150 km.

1. INTRODUCTION

The Central Taurides mountain range runs along the Mediterranean coast of central Turkey (Fig. 1) and forms the 2–3-km-high southern rim of the Central Anatolian Plateau. The southern Central Taurides are unconformably covered by Miocene–Pleistocene marine sedimentary rocks of the Mut Basin, which reaches ~2 km elevation and records multiple phases of km-scale subsidence and uplift since ca. 8 Ma (e.g., Cosentino et al., 2012; Öğretmen et al., 2018). The stratigraphy of the Mut Basin is undeformed (e.g., Fernández-Blanco et al., 2019), leading to the interpretation that km-scale uplift was driven by deep processes related to the underlying Cyprus subduction zone (e.g., Schildgen et al., 2012; Schildgen et al., 2014). The region is therefore considered a potential location in which we may study the interplay between subduction dynamics and rapid surface uplift and subsidence (e.g., Schildgen et al., 2014; Delph et al., 2017; Meijers et al., 2018). The specific causes of uplift in the southern Central Taurides, and whether the uplift history represents regional-scale rise of the Central Anatolian Plateau, remain uncertain.

The Central Taurides comprise a Late Cretaceous to late Eocene forearc fold-thrust belt, which formed in the upper plate of the Cyprus and Antalya subduction zones (McPhee et al., 2018a, 2018b). The Central Anatolian Plateau interior corresponds to a Late Cretaceous to middle Eocene backarc extensional province (Gürer et al., 2018b) that was active during the formation of the Taurides forearc fold-thrust belt, and is characterized by a kilometer-high average elevation, low topographic relief, and an extensive internal drainage system. The modern morphology of the Central Anatolian Plateau—a high elevation forearc fold-thrust belt with a low-elevation backarc region—is typical of many active subduction zones across the Mediterranean region, such as the Carpathian-Pannonian, Aegean, Apennine-Tyrrhenian, or Betic-Rif-Alboran regions (e.g., Royden and Faccenna, 2018). This raises the question: was the modern plateau morphology inherited from the physiography of the Eocene and older subduction zone? Answering this question is crucial if we are to isolate the signature of Miocene to recent geodynamics in the rise of the plateau.

The Eocene–Miocene history of the Central Taurides remains subject to many uncertainties, in part because subduction from this time period left no known stratigraphic or accretionary record in southern Turkey. As rock uplifts, surface uplift tends to be moderated by denudation, resulting in the upward transport of rock toward the surface. This transported rock cools, and the history of this cooling may be captured by low-temperature thermochronometers (e.g., Reiners and Brandon, 2006; Peyton

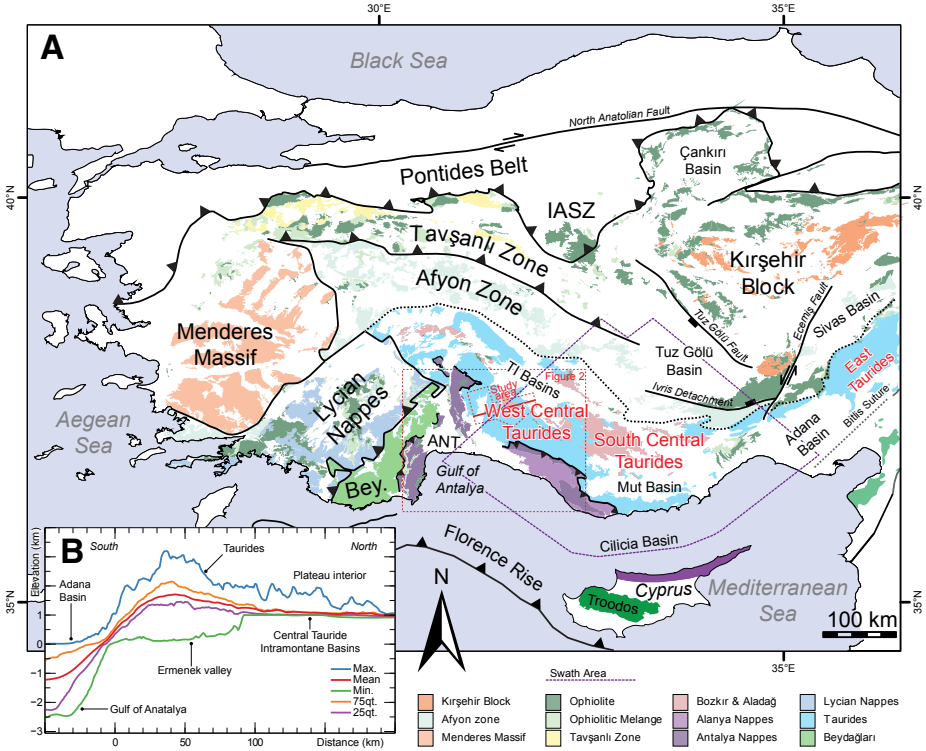

Figure 1. (A) Major fault zones and tectonostratigraphic units of Turkey. Red dashed box indicates the study area in which we collected our samples. TI Basins—Tauride intramontane basins; ANT—Antalya Basins; Bey.—Beydaglari Platform; IASZ—Izmir-Ankara Suture Zone. (B) Elevation swath taken across the Taurides, which highlights the high-elevation plateau margin and lower-elevation plateau interior.

and Carrapa, 2013). In the absence of a stratigraphic record, we use thermochronometers to reconstruct the thermal history of rock samples. From this thermal history, we aim to infer the long-term history of erosional exhumation of the fold-thrust belt. To this end, we collected rock samples and used zircon (U-Th)/He (ZHe), apatite (U-Th)/He (AHe), and apatite fission-track (AFT) thermochronometers, which record cooling through <200 °C, typically corresponding to exhumation from the upper kilometers of the crust. We focus on the western Central Taurides, where we have good structural and stratigraphic control on the architecture of the orogen (McPhee et al., 2018a), and we interpret our results using inverse thermal modeling. We discuss our interpretations in terms of the long-term evolution of vertical motions in the Central Anatolian Plateau region, in the context of Eastern Mediterranean subduction.

2. SETTING

2.1 Crustal Architecture of the Central Anatolia Plateau

Central Anatolia contains a broad orogenic belt that stretches east-west across Turkey (Fig. 1). This Anatolian orogen formed largely in Late Cretaceous–Eocene time and is bound in the north by the Izmir Ankara suture zone (IASZ). The orogen is made of a series of continent- and oceanic-derived crustal blocks (the Kırşehir block and Tavşanlı zone; and the Afyon Zone), which were accreted with overall south-younging ages of climax metamorphism and thrusting (Şengör and Yilmaz, 1981; van Hinsbergen et al., 2010; Pourteau et al., 2010; van Hinsbergen et al., 2016; Gürer et al., 2018a). These continent-derived crustal blocks are covered by klippen of ca. 94–90 Ma (Upper Cretaceous) supra-subduction zone (SSZ) ophiolite and ophiolitic mélange, which form the highest structural units in the Anatolian orogen (Dilek et al., 1999; Robertson, 2004; Pourteau et al., 2010; van Hinsbergen et al., 2016). The ophiolites are interpreted as remnants of an ocean lithosphere upper plate, which was located above a north- and east-dipping subduction zone. The mantle lithospheric underpinnings of the continent-derived blocks were subducted (van Hinsbergen et al., 2016), and their (upper) crust was accreted and metamorphosed. The metamorphic rocks were then extensionally exhumed in a latest Cretaceous to early Eocene backarc region, which occupied much of what is now the modern plateau interior (Gürer et al., 2018b; see also Seyitoğlu et al., 2017).

The Late Cretaceous–Eocene Taurides fold-thrust belt forms the high southern margin of the Central Anatolian Plateau. The Taurides are the southernmost and youngest accreted unit exposed in Anatolia and escaped deep burial and metamorphism (Özgül, 1984; McPhee et al., 2018a). In our focus area of the western Central Taurides, they comprise three major nappes (Fig. 1). The highest of these is the composite Bozkır nappe, which contains the previously mentioned Cretaceous SSZ ophiolites, sub-ophiolitic mélange, as well as km-scale blocks of deformed Triassic to Upper Cretaceous shelf and platform–margin carbonates (Özgül, 1976; Gutnic et al., 1979; Andrew and Robertson, 2002). The far-traveled Aladağ and Bolkardağı nappes (to which the metamorphosed Afyon Zone belongs) form the next structural units of the belt and contain Paleozoic to Upper Cretaceous platform carbonates, which are overlain by thin Upper Cretaceous synorogenic rocks (Özgül, 1984; Altiner et al., 2000). In our study area, the Bolkardağı nappe is absent.

The Geyikdağı nappe is the next structural unit and is the main focus of our study. The Aladağ and Bolkardağı nappes, and overlying Bozkır nappes, were thrust at least 70 km southwestward over the Geyikdağı nappe, as shown by tectonic windows and klippen (McPhee et al., 2018a). McPhee et al. (2018a, 2018b) observed that the Geyikdağı nappe is internally deformed and interpreted a thin-skinned style of thrusting based on widespread flat-on-flat thrust contacts, tectonic windows and re-entrants, and klippen. This thrusting produced the Derebucak thrust imbricate toward the foreland (west) and a duplex that is enveloped by the Seydişehir anticline toward the hinterland (east) (Fig. 2). Thrusting of the Aladağ and Bozkır nappes over the Geyikdağı nappe, as well as thrusting within the Geyikdağı nappe was active in the middle Eocene (ca. 40 Ma) based on the youngest synorogenic stratigraphy involved in thrusting (Gutnic et al., 1979). Structural restorations suggest that internal thrusting in the Geyikdağı nappe was associated with only several tens of kilometers of shortening, which, given Eocene Africa-Europe convergence rates of ~3–4 cm/yr, could have taken place in a few million years in the middle Eocene (ca. 40 Ma) (McPhee et al., 2018a).

The lowest structural unit in the belt is the Beydağları platform, which forms the foreland of the western Central Taurides. The Beydağları platform is interpreted as the former western extension of the Geyikdağı platform, which escaped internal thrust imbrication (Gutnic et al., 1979). Structural constraints suggest the Beydağları platform was underthrusted below the Geyikdağı nappe by a minimum of a few kilometers in Eocene time (McPhee et al., 2018a). On the other hand, palinspastic restorations that incorporate paleomagnetic constraints suggest up to some tens of kilometers of Eocene underthrusting (McPhee et al., 2018b).

An added complexity of the Tauride geology is that in latest Cretaceous time, the Beydağları-Geyikdağı platform was overthrusted by a separate, older, south-derived nappe stack known as the Antalya-Alanya nappes. These nappes were emplaced from south to north onto the platform by Paleocene time (Özgül, 1984) and were incorporated into the younger top to the S(W) fold-thrust belt during the Eocene north to south thrusting described above. So far, the only published low-temperature thermochronometric data in the region are AFT cooling ages recovered from the Alanya nappes, to the southeast, and structurally above the Geyikdağı nappe. Cooling ages of ca. 29–32 Ma (early Oligocene) are reported (Mittiga, 2015), but no track length data are reported, making these ages difficult to interpret.

After the final assembly of the Taurides in Eocene time, Africa-Eurasia plate convergence continued. Plate circuit constraints show that >500 km of plate convergence occurred since Eocene time, which must largely have been accommodated by subduction on a trench located to the south of the Taurides and by shortening within the Anatolian orogen (Gürer and van Hinsbergen, 2019). The precise location of the subduction zone to the south of Anatolia, however, remains controversial (e.g., Barrier and Vrielynck, 2008; McPhee and van Hinsbergen, 2019). There is no known sedimentary record for the structural or morphological evolution of the western Central Taurides, until deposition of the lower Miocene–Pliocene mostly marine sediments in the Antalya Basin (e.g., Ciner et al., 2008).

The Antalya Basin contains stratigraphic (Karabiyikoğlu et al., 2000; Deynoux et al., 2005; Poisson et al., 2011) and possible structural evidence (McPhee et al., 2018a) for N-S–trending normal faults that were active in the early Miocene. After that, the Antalya Basin was deformed by a new phase of west-verging thrusting and folding, mostly concentrated in the western Taurides, since at least middle Miocene time, until Pliocene times (Poisson et al., 2003; Koç et al., 2016; McPhee et al., 2018a, based on the age of rocks incorporated in thrust sheets (Ciner et al., 2008) and in the footwalls of thrusts (Poisson et al., 2003). This E-W shortening is not regional; instead, it is associated with westward-convex oroclinal bending in the western Central Taurides (Koç et al., 2016). Tens of kilometers of associated shortening (McPhee et al., 2018a) are kinematically balanced by E-W extension in the Tauride intramontane basins in the hinterland area of the western Central Taurides (Koç et al., 2018) (Fig. 1).

Seismic tomography of the mantle below Anatolia shows two separate bodies, the NW-SE–striking Antalya slab in the southwest and the E-W–striking Cyprus slab in the southeast (Biryol et al., 2011; van der Meer et al., 2018). These slabs are widely viewed as a once contiguous subducted lithosphere broken in Miocene time (e.g., Schildgen et al., 2014), but McPhee et al. (2018a) recently argued that the two bodies had been separated already in Eocene time, whereby the Antalya slab was disconnected from the African plate during the accretion of the Beydağları platform to the upper plate. If correct, the upper-mantle portion of the Cyprus slab consists mainly of oceanic crust subducted after the Eocene, and the Antalya slab is a dangling continental lithospheric slab that subducted in the Eocene and failed to detach. Recent seismological evidence suggests that the Cyprus slab may have largely detached, probably in Plio-Pleistocene time (Portner et al., 2018).

2.2 Constraints on Taurides Erosion and Deposition from the Evolution of the Antalya Basin

The marine to marginal-marine Antalya Basin (Figs. 1 and 2) was unconformably deposited onto the deformed and eroded Taurides and Antalya-Alanya nappes. The depositional record of the Antalya Basin starts with Aquitanian (ca. 23–20 Ma) shallow-water limestones that cover Antalya nappes rocks around Sutçuler and Şerik (Akbulut, 1977; Poisson et al., 1983; Flecker et al., 2005) (Fig. 2). Elsewhere, Aquitanian–Burdigalian (ca. 23–16 Ma) conglomerates have been reported in the Aksu-1 and Manavgat 1 and 2 boreholes (Fig. 2) (Poisson et al., 2011; Hall et al., 2014). Similar rocks are found unconformably overlying the Tauride units in the Mut Basin.

In the Köprüçay and Manavgat basins (Fig. 2), the oldest dated rocks are the Burdigalian–Langhian (ca. 20–14 Ma) Oymapınar Limestone Formation, which in places covers a basal conglomerate of an undetermined age (Karabiyikoğlu et al., 2000; Deynoux et al., 2005). The basal conglomerate contains pebbles that are likely derived from the Bozkır nappes that form the highest structural unit of the Taurides (Monod and Kuzucuoğlu, 2019). The drainage system that delivered those pebbles may be preserved as abandoned paleovalleys that cut

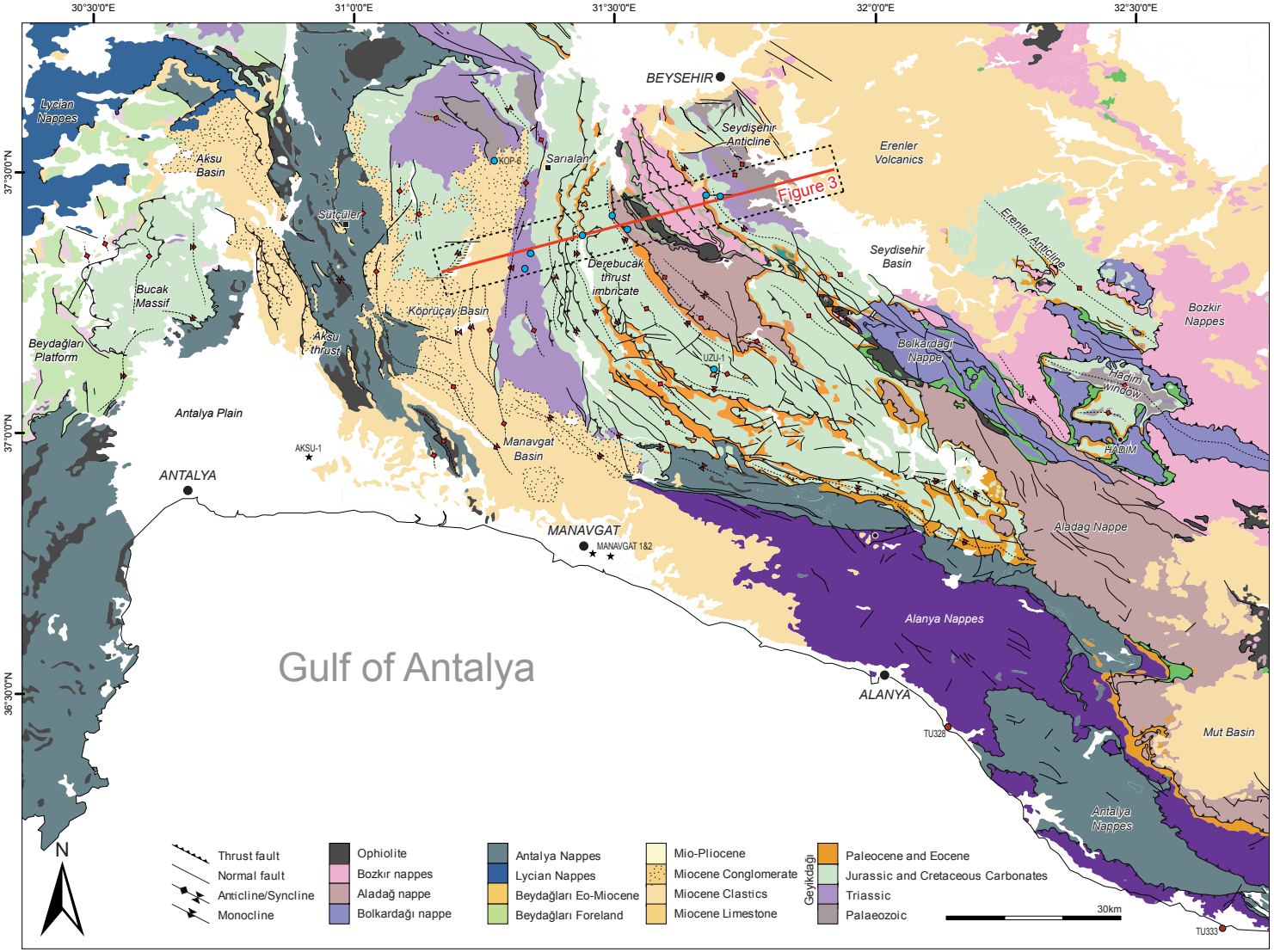

Figure 2. Geological map of the western Taurides showing generalized geological units and major faults and folds, adapted from the General Directorate of Mineral Research and Exploration (MTA) 1:500,000 Scale Geological Inventory Map Series of Turkey. The extent of the strip map in Figure 3A is shown by the black dashed box. The cross section in Figure 3B is shown by the red line. Blue points are sample locations in this study: point UZU-1 marks a sample location in the Üzümdere Valley, and KOP-6 marks a sample location in the northern Köprüçay Valley. Red points (TU328 and TU333) are locations of apatite fission-track cooling ages from Mittiga (2015). Black star symbols are Borehole Aksu-1; and Manavgat 1 and 2 are reported in Hall et al. (2014) and Poisson et al. (2011).

into a low-relief surface defined by mountain peaks, which has an inferred early Miocene age, based on lower Miocene sediments that may be associated with them (Monod et al., 2006). The conglomerates fill a paleo-topography and form fans that were deposited in subaerial to shallow marine conditions (Karabiyikoğlu et al., 2000). The Oymapınar Limestone broadly consists of a deepening-upwards shallow-marine carbonate shelf succession (Karabiyikoğlu et al., 2000). Deposition of that limestone was widespread in the Köprüçay and Manavgat subbasins, where it is now preserved at up to ~1 km and ~1.5 km above sea level, respectively (Fig. 2).

In Langhian–Serravallian times (ca. 16–11 Ma), marine sandstone and marl of the Karpuzçay Formation covered (and in places are shown to onlap) the Oymapınar Limestone and are thought to represent continued relative sea-level rise (Deynoux et al., 2005; Flecker et al., 2005; Ciner et al., 2008). In the Köprüçay and Aksu subbasins, deposition of the upper Karpuzçay Formation was accompanied by significant conglomerate deposition (Deynoux et al., 2005). Messinian rocks are absent from the northern parts of the Köprüçay Basin, except for lower Messinian (ca. 7 Ma) marine marl at Sarıalan (preserved at ~1400 m above sea level), which constrains the maximum age for onset of Miocene surface uplift in the western Central Taurides (Schildgen et al., 2012).

The Antalya Basin was affected by a Messinian unconformity, after which there is no sedimentary record in the northern, higher-elevation parts of the basin. Pliocene marine sedimentary rocks as young as uppermost lower Zanclean (ca. 3.5 Ma) (Glover and Robertson, 1998) are reported in the southernmost low-elevation parts of the basin (<100 m above sea level) and as far north as Kargı in the Aksu Basin (300 m above sea level) (Poisson et al., 2003). Those sedimentary rocks are covered by terrestrial tufa deposits that indicate emergence of the basin (Glover, 1995).

2.3 Modern Geothermal Gradient

Data for the modern geothermal gradient in the region may be used to roughly estimate past thermal conditions. These data, however, are sparse, and no borehole data are available for the study area. The best constraint we have comes from deep boreholes in the Beydağları platform, which is laterally equivalent to the Geyikdağı nappe. Demirel et al. (2001) reported borehole temperatures from wells there that suggest a modern geothermal gradient of 22–32 °C/km through carbonate rocks and 48 °C/km through Kasımlar Formation sandstone and shales (Fig. 2). They observed that the modern geothermal gradient is strongly disrupted or inverted by meteoric water circulation localized around fault zones.

3. METHODS

We aimed to use zircon (U-Th)/He (ZHe), apatite (U-Th)/He (AHe), and apatite fission-track (AFT) low-temperature thermochronometers to constrain the time-temperature history of rock samples from the western Central Taurides. These thermochronometers typically record the thermal evolution of rocks in the upper few kilometers of the crust.

We collected samples of sandstone along the line of the NNE-SSW–trending Bucak-Seydişehir structural cross section of McPhee et al. (2018a) (Figs. 2 and 3). Additional samples were collected from the Üzümdere Valley and northern Köprüçay Valley (Fig. 2). The stratigraphy of the Taurides is dominated by carbonate rocks that lack apatite and zircon, and so our sampling choices were limited to rare sandstone intervals. Standard magnetic and heavy liquid separation techniques were used to separate apatite and zircon grains from all samples (at Zirchron LLC, Tucson, Arizona). Eight samples yielded apatite, and nine samples yielded zircon.

3.1 He Dating

AHe and ZHe thermochronometers rely on the temperature sensitivity of diffusion of radiogenic helium. In addition to temperature, helium diffusion is controlled by grain size (e.g., Farley, 2000), accumulated radiation damage (e.g., Shuster et al., 2006), and zonation of U and Th (and Sm) (e.g., Meesters and Dunai, 2002).

The effective closure temperature is defined as the temperature of the dated mineral at the time indicated by the thermochronometric cooling age (Dodson, 1973) and is dependent on cooling rate, accumulated radiation damage, and He diffusion kinetics. The effective closure temperature of the AHe system varies between ~30 °C and ~90 °C (Flowers et al., 2009). For the ZHe system, the effective closure temperature typically varies between ~130 and 200 °C, and at extremely high alpha doses, the closure temperature may be considerably lower (Guenthner et al., 2013).

Accumulated radiation damage affects He diffusivity in apatite and zircon. High levels of accumulated radiation damage in apatite increase He retention and hence raise the effective closure temperature (e.g., Shuster et al., 2006; Shuster and Farley, 2009). In zircon, low levels of radiation damage increase He retention, and at high levels of damage, reduce retention, raising and lowering the effective closure temperature, respectively (e.g., Reiners et al., 2004; Guenthner et al., 2013). Variations in accumulated radiation damage may therefore lead to dispersed helium ages, particularly in rocks that cool slowly. Effective uranium (eU) content may be used as a proxy for radiation damage, and so He age dispersion caused by accumulated radiation damage should yield a positive correlation between He age and eU (e.g., Flowers et al., 2009).

AHe and ZHe analyses were conducted at the Arizona Radiogenic Helium Dating Laboratory at the University of Arizona. We picked single-grain aliquots of apatite and zircon with a minimum width greater than 60 μm and no visible inclusions. Analysis followed standard procedures described in Reiners et al. (2004) and Guenthner et al. (2016). Single grains were placed in niobium tubes and then degassed individually by laser heating. He content was measured using ^{3}He isotope dilution, cryogenic purification, and quadrupole mass spectrometry. Degassed grains were dissolved, and U-Th-Sm content of each grain was measured using inductively coupled plasma mass spectrometry. He ages are reported as raw ages and α-ejection corrected ages following the age correction approach of Ketcham et al. (2011) and assuming a uniform distribution of parent nuclides.

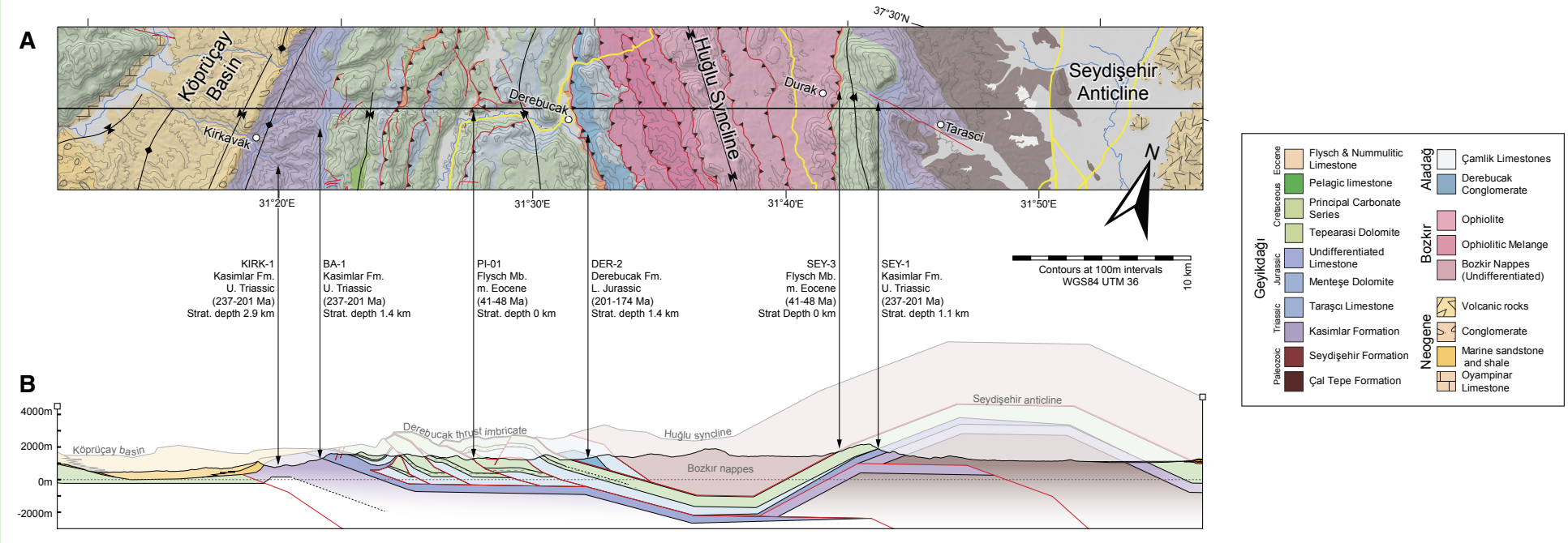

Figure 3. (A) Geological strip map of the western Taurides modified from McPhee et al. (2018a), showing sample locations along the Bucak-Seydişehir cross section. (B) ENE segment of the Bucak-Seydişehir cross section (McPhee et al., 2018a), showing sample locations.

3.2 AFT Dating

AFT thermochronometry relies on the time and temperature sensitivity of annealing of fission tracks: damage in the crystal lattice created by the radioactive decay of U^{238}. The effective closure temperature (annealing temperature) of the AFT thermochronometry is dependent on cooling rate and the kinetics of track annealing, which are controlled primarily by time and temperature, and secondarily by variable apatite composition and crystallographic anisotropy (e.g., Green et al., 1986; Ketcham et al., 2006). At temperatures below the closure temperature (~110 °C at a cooling rate of 10 °C/m.y.; e.g., Ketcham et al., 1999), fission tracks are preserved, and their abundance may be used to date cooling through the annealing zone.

Apatite fission-track analysis was conducted at the University of Arizona Fission Track Laboratory. Apatite grains were mounted in epoxy and were polished, and spontaneous fission tracks were revealed by etching with 5.5 M HNO_3 at 20 °C for 20 seconds. Samples were analyzed following the external detector method using very low uranium, annealed muscovite mica detectors; the samples were then irradiated at the Oregon State University TRIGA Reactor, Corvallis, Oregon, USA. The neutron fluence was monitored using European Institute for Reference Materials and Measurements (IRMM) uranium-dosed glass IRMM 540R. After irradiation, induced tracks in the mica external detectors were revealed by etching with 48% HF for 20 minutes. Spontaneous and induced FT densities were counted using an Olympus BX61 microscope at 1250× magnification with automated Kinetek Stage system. Apatite FT lengths and Dpar values were measured using FTStage software, an attached drawing tube, and digitizing tablet supplied by Trevor Dumitru of Stanford University; the tablet was calibrated against a stage micrometer. Central ages (Galbraith and Laslett, 1993) were calculated according to the International Union of Geological Sciences (IUGS)–recommended zeta-calibration approach of Hurford and Green (1983) using an apatite IRMM 540R zeta-calibration factor of 368.1 ± 14.9.

4. RESULTS

We describe our results on a sample-by-sample basis. AHe results are shown in Table 1. A summary of AFT results is shown in Table 2, and

TABLE 1. APATITE (U–Th)/He DATA

Sample	Rs (μm)	Mass (μg)	U (ppm)	Th (ppm)	Sm (ppm)	eU (ppm)	Th/U	He^4 (nmol/g)	Raw age (Ma)	σ1 (Ma)	FT	Corrected age (Ma)	σ1 (Ma)
KOP-6													
1	74.4	5.17	18.7	1.8	151.5	19.1	0.1	1.0	17.9	0.4	0.819	21.9	0.5
2	72.0	5.84	1.9	3.1	9.6	2.7	1.7	1.1	76.4	1.4	0.801	*95.4	1.7
3	73.3	1.38	5.4	4.5	152.8	6.4	0.9	0.3	7.5	0.3	0.826	*9.1	0.4
4	69.2	2.39	24.0	10.9	406.1	26.6	0.5	1.9	13.3	0.3	0.810	*16.4	0.4
5	71.8	5.90	9.9	3.8	81.6	10.8	0.4	1.0	17.0	0.4	0.810	21.0	0.5
BA-1													
1	51.9	1.94	4.9	18.9	65.5	9.3	4.0	0.7	12.8	0.6	0.720	17.8	0.8
2	49.6	1.68	26.2	93.8	332.3	48.3	3.7	2.9	11.1	0.2	0.708	15.7	0.3
3	45.8	1.43	5.8	21.6	265.7	10.9	3.8	0.8	13.6	0.6	0.710	19.1	0.8
4	46.6	2.26	6.3	95.6	59.8	28.8	15.4	1.4	9.2	0.2	0.665	13.8	0.3
5	55.8	2.66	16.5	148.0	222.9	51.3	9.2	2.2	7.7	0.2	0.727	10.6	0.3
DER-2													
1	67.0	7.39	27.6	80.4	218.2	46.5	3.0	6.1	23.9	0.4	0.782	30.6	0.5
2	37.0	1.17	45.6	98.1	575.4	68.7	17.0	7.2	19.1	0.3	0.623	30.7	0.5
3	50.5	2.71	8.0	132.5	472.8	39.1	12.2	12.3	57.0	1.1	0.706	*80.7	1.6
4	49.6	1.99	10.4	123.9	484.6	39.5	3.0	4.3	19.7	0.4	0.701	28.1	0.6
5	72.8	7.68	13.2	38.0	405.4	22.1	2.2	2.4	19.8	0.4	0.813	24.4	0.5
KIRK-1													
1	31.9	0.92	6.1	13.1	111.7	9.2	2.2	0.4	8.9	0.4	0.574	15.5	0.7
2	34.3	0.81	82.0	8.1	468.8	83.9	0.1	5.2	11.4	0.3	0.608	18.7	0.5
3	48.4	2.15	16.8	34.3	317.4	24.8	2.1	1.4	10.1	0.3	0.716	14.1	0.4
4	46.8	1.53	7.2	30.9	73.0	14.5	4.4	1.7	22.0	0.6	0.686	*32.1	0.9
5	38.0	0.94	41.8	121.5	107.0	70.3	3.0	3.4	8.9	0.2	0.614	14.5	0.3
6	55.0	2.82	7.6	41.0	208.4	17.2	5.5	1.3	14.2	0.4	0.739	19.2	0.5
SEY-3													
1	50.9	2.30	9.2	24.6	412.3	15.0	2.7	2.6	31.3	0.7	0.746	*42.0	0.9
2	42.1	1.75	2.0	19.0	32.8	6.5	9.5	0.5	12.8	0.7	0.642	20.0	1.1
3	44.0	1.55	21.9	38.7	506.5	31.0	1.8	3.0	17.7	0.4	0.695	25.5	0.6
4	41.7	1.72	2.5	17.2	316.4	6.6	7.0	0.5	12.6	1.1	0.706	17.8	1.6
5	36.0	0.87	5.6	76.7	418.4	23.6	14.1	1.6	12.1	0.7	0.606	20.0	1.2
SEY-1													
1	46.4	1.56	1.2	16.1	10.9	5.0	13.8	0.2	5.6	0.3	0.665	*8.43	0.5
2	43.5	1.42	2.9	38.4	90.5	11.9	13.5	0.7	10.7	0.9	0.654	16.4	1.4
3	—	0.59	6.4	50.4	42.4	18.2	8.1	0.7	7.4	0.2	—	—	—
4	49.0	1.75	11.8	38.8	51.5	20.9	3.4	1.8	15.8	0.4	0.698	22.6	0.6
5	36.1	0.95	3.6	64.5	23.3	18.8	18.3	0.6	5.9	0.3	0.568	10.4	0.5

*AHe ages omitted from inverse modelling.
FT—effective α-ejection correction factor (calculated in HeFTy, v. 1.9.3; Ketcham, 2005).

sample-by-sample AFT data are included in the Supplemental File[1]. ZHe results are shown in Table 3. Age–effective uranium (eU) and age–grain-size plots of AHe and ZHe data are included in the Supplemental File. In general, the apatite grains were subrounded, and their surfaces were frosted, reflecting the fact that they were taken from sedimentary rocks. In the AFT analysis, owing to low apatite yield and low track densities, only sample DER-2 contained confined tracks for measurement.

KOP-6

This sample was taken from Precambrian sedimentary rocks in the northern part of the Köprüçay Valley (Fig. 2). These rocks are unconformably covered by both an Upper Triassic to Upper Cretaceous stratigraphy and Langhian (13.7 Ma) and younger conglomerates. An AFT age of ca. 22 Ma was measured from a population of grains with low age dispersion. We measured AHe ages in five grains. Two grains contained low calcium (549 and 951 ng) and low eU (1.8 and 5.6 ppm) and were therefore unlikely to be apatite; thus these grains were excluded from further analysis. A third grain contained a low concentration of eU (2.7 ppm) and yielded a ca. 97 Ma age, which in light of the AFT age, we treated as an outlier. The remaining two grains had an arithmetic mean age of ca. 22 Ma.

KIRK-1

This sample was taken from the Upper Triassic Kasımlar Formation (ca. 237–201 Ma) in the core of the Kirkavak anticline (Fig. 3). We measured three ZHe single-grain ages of ca. 38 Ma, ca. 49 Ma, and ca. 51 Ma and an AFT age of ca. 24 Ma. We measured AHe ages in six grains, with ages ranging from ca. 14 Ma to ca. 19 Ma. In light of the AFT results, we treated an AHe age of ca. 32 Ma as an outlier. AHe data showed no strong age-eU or age–grain-size correlation.

BA-1

This sample was taken from the uppermost stratigraphy of the Upper Triassic Kasımlar Formation (ca. 237–201 Ma), in the eastern limb of the Kirkavak anticline, and stratigraphically above sample KIRK-1 (Fig. 3). We measured an AFT age of ca. 25 Ma, within error of the nearby KIRK-1 sample. AHe ages were measured in five grains and ranged from ca. 11 Ma to ca. 19 Ma. A negative age-eU correlation suggested that dispersion was caused by an additional process such as implantation of helium from outside the grain or strong zonation of parent nuclides.

Supplementary file 01

McPhee, P.J., van Hinsbergen, D.J.J., and Thomson., S.

Figure S1 and S2 show age vs. effective uranium and age vs. grain size plots for AHe and ZHe results respectively.

Table S1 to S8 contain individual grain ages and compositions from AFT analysis. In addition, Table S2 contains fission track length data.

Table S9 contains vitrinite reflectance data from Hokerek et al., (2014), used in inverse thermal modelling of sample KOP-6.

Figures S3 to S8 show results of inverse thermal modelling shown in Figure 4 of the main article, plus pre-100 Ma time-temperature paths. Constraint boxes are shown in thin blue lines; good-fitting paths are pink; acceptable-fitting paths are green; weighted mean path is navy-blue. Path generation criteria are shown in white boxes. Tables in each figure show model ages and measured ages for best fitting model paths (thick black lines).

[1]Supplemental File. Apatite fission-track data tables and radial plots, age versus effective uranium and age versus grain size plots of AHe and ZHe data, and inverse thermal models showing results and constraint boxes beyond 100 Ma. Please visit https://doi.org/10.1130/GES02164.S1 or access the full-text article on www.gsapubs.org to view the Supplemental File.

TABLE 2. APATITE FISSION-TRACK DATA

Sample number	No. of crystals	Track density ($\times 10^6$ tracks.cm^{-2}) (Number of tracks) ρ_s (N_s)	ρ_i (N_i)	ρ_d (N_d)	Mean Dpar (μm)	Age dispersion ($P\chi^2$)	Central age (Ma) (±1σ)	Apatite mean track length (μm ± 1 s.e.) (no. of tracks)	Standard deviation (μm)
SEY-1	13	0.2096 (44)	1.096 (230)	1.274 (4076)	2.13	<0.01% (99.5%)	**44.7 ± 7.6**	-	-
SEY-3	20	0.1743 (120)	0.5518 (380)	1.264 (4045)	2.47	0.19% (81.3%)	**73.1 ± 8.3**	-	-
BA-1	16	0.2182 (75)	1.999 (687)	1.254 (4013)	2.11	<0.01% (98.6%)	**25.2 ± 3.3**	-	-
PI-01	6	0.0801 (8)	0.1402 (14)	1.244 (3982)	2.41	3.07% (55.0%)	**129.4 ± 57.7**	-	-
KIRK-1	12	0.2579 (34)	2.458 (324)	1.235 (3951)	2.09	<0.01% (99.9%)	**23.8 ± 4.4**	-	-
UZU-1	5	0.1192 (18)	1.265 (191)	1.225 (3920)	2.08	<0.01% (72.8%)	**21.2 ± 5.3**	-	-
DER-2	20	0.2374 (218)	0.5891 (541)	1.215 (3889)	2.48	32.3% (2.0%)	**89.5 ± 10.7 mixed age**	**11.65 ± 0.65 (8)**	**1.71**
KOP-6	20	0.2438 (118)	2.462 (1193)	1.206 (3858)	2.04	<0.01% (99.9%)	**21.9 ± 2.3**	-	-

Notes: Analyses by external detector method using 0.5 for the 4π/2π geometry correction factor. Ages calculated using dosimeter glass: IRMM540R with ζ_{540R} = 368.1 ± 14.9 (apatite). $P\chi^2$ is the probability of obtaining a χ^2 value for v degrees of freedom where v = no. of crystals − 1. s.e.—standard error of the mean.

PI-01

Sample PI-01 was taken from Eocene synorogenic rocks (ca. 41 Ma) in the footwall of a thrust fault (Fig. 3). The quality and yield of apatite were low, and so we did not conduct AHe analysis. We measured an AFT age of ca. 129 Ma based on eight grains.

UZU-1

Sample UZU-1 was taken from Lower Jurassic rocks (201–174 Ma) exposed in a tectonic window through the Derebucak thrust sheet, close to the village of Üzümdere (Fig. 2), ~60 km along strike of the Bucak-Seydişehir cross section. The sample had a ca. 21 Ma AFT age. Single-grain ages were younger than the stratigraphic age of the sample and had low age dispersion. The quality and yield of apatite were low, and so we did not conduct AHe analysis.

TABLE 3. ZIRCON (U–Th)/He DATA

Sample	Rs (μm)	Mass (μg)	U (ppm)	Th (ppm)	eU (ppm)	Th/U	He^4 (nmol/g)	Raw age (Ma)	σ1 (Ma)	FT	Corrected age (Ma)	σ1 (Ma)
KIRK-1												
1	42.2	2.56	245.9	95.7	268.4	0.4	53.3	36.7	1.0	0.723	50.8	1.4
2	45.3	1.94	527.7	174.3	568.7	0.3	110.7	36.0	1.0	0.742	48.5	1.3
3	52.1	4.46	287.0	331.7	365.0	1.2	58.2	29.5	0.8	0.770	38.3	1.0
SEY-1												
1	50.3	4.09	336.3	62.9	351.1	0.2	498.1	257.2	7.0	0.773	332.6	9.1
2	44.1	1.94	421.2	169.0	460.9	0.4	417.4	165.6	4.4	0.738	224.5	6.0
3	54.1	3.26	303.4	100.6	327.0	0.3	346.5	193.2	3.1	0.787	245.6	3.9

FT—effective α-ejection correction factor (calculated in HeFTy, v. 1.9.3; Ketcham, 2005).

DER-2

This sample was taken from Lower Jurassic (201–174 Ma) sandstone of the Aladağ nappe (Fig. 3). Apatite grains from this sample contained eight confined fission tracks with a mean track length of 11.65 μm. Measured single grain ages were dispersed, with some ages older than the depositional age of the sample, suggesting partial resetting. AHe ages were measured from five grains. Four grains showed a positive age-eU correlation and low age dispersion (<10%), and had an arithmetic mean age of ca. 29 Ma. We measured an outlying ca. 82 Ma AHe age in one grain.

SEY-3

This sample was taken from Eocene synorogenic rocks (ca. 40 Ma) on the western limb of the Seydişehir anticline, structurally below the Bozkır nappes (Fig. 3). An AFT age of ca. 73 Ma was measured. The majority of single-grain AFT ages were older than the stratigraphic age of the sample, with some ages close to or younger than the stratigraphic age of the sample. We measured AHe ages in five grains. Four grains had ages ranging from ca. 18 Ma to ca. 26 Ma, and a fifth grain had an outlying AHe age of ca. 42 Ma. A positive age-eU and age–grain-size correlation was observed for these data.

SEY-1

This sample was taken from Upper Triassic rocks of the Kasımlar Formation (ca. 237–201 Ma) on the western limb of Seydişehir anticline, 1 km stratigraphically below sample SEY-3, but at a slightly higher elevation due to bedding dip (Fig. 3). We measured three ZHe single-grain ages of ca. 225 Ma, ca. 246 Ma, and ca. 333 Ma in this sample. An AFT age of ca. 45 Ma was measured. AHe ages

were measured in five grains from sample SEY-1. Helium ages between ca. 8 Ma and ca. 23 Ma were measured in four grains. One grain lacked grain-size measurements, and therefore an α-ejection correction was not possible. The youngest helium age was measured in a grain with a low eU concentration (1.2 ppm). AHe data showed a weak positive age-eU and age–grain-size correlation.

5. INTERPRETATIONS

Inverse Modeling

We measured dispersed cooling ages, and potentially some partially reset ages in our samples. We used an inverse modeling approach on a sample-by-sample basis in the software package HeFTy 1.9.3 (Ketcham, 2005) to investigate the range of thermal histories that may reproduce our thermochronometric data (Fig. 4). HeFTy generates a large number of random time-temperature paths and predicts cooling ages for inputted grain data (composition and equivalent spherical grain size). The misfit between measured cooling ages and modeled cooling ages is then analyzed. Time-temperature paths that are supported by the data are defined as having a *good fit* (goodness of fit ≥ 0.5), and paths that are not ruled out by the data are defined as having an *acceptable fit* (0.5 > goodness of fit ≥ 0.05), according to statistical tests described in Ketcham (2005; see also Vermeesch and Tian, 2014). The parameters used in our modeling are detailed in Table 4.

Geological time-temperature constraints (stratigraphic ages, nappe emplacement, and known unconformities) were enforced on the model space as *constraint boxes.* All randomly generated time-temperature paths were forced to pass through these boxes.

In sedimentary rocks, radiation damage may be inherited from a pre-depositional history if damage is not annealed by reheating. We accounted for the effects of radiation damage in two ways: (1) we used kinetic models that accounted for the effects of accumulated radiation damage in apatite (Flowers et al., 2009) and zircon (Guenthner et al., 2013); and (2) we defined pre-depositional *constraint boxes* to simulate uncertainty about the pre-depositional history of grains. These boxes also accounted for the potential effects of partial retention of helium due to partial resetting.

KOP-6

An early Miocene cooling age was found in both AHe and AFT analyses, suggesting rapid cooling at that time. In thermal modeling, we tested pre-Paleocene heating due to emplacement of the Antalya nappes because this nappe stack is presently exposed to the north of the sample location (Fig. 2).

We modeled vitrinite reflectance data and thermochronometric data separately but simultaneously and assumed that the vitrinite was of Late Triassic origin. We imposed a burial constraint box that represented the maximum (~3 km) stratigraphic overburden in Maastrichtian times (72–66 Ma), prior to tectonic burial below the Antalya nappes. We also imposed a constraint box that represented surface exposure of the sample prior to burial below Langhian (13.7 Ma) and younger conglomerates.

High temperatures (190–240 °C for good-fitting paths) in Late Cretaceous times were required to reproduce vitrinite reflectance data from the overlying Triassic rocks, requiring burial below a thick Antalya nappes overburden. The vitrinite samples were taken over a large stratigraphic interval, likely ruling out inclusion of reworked material. We ran models without vitrinite reflectance data and found that paths were unaffected where constrained by AFT and AHe data. We found that rapid cooling (>>10 °C/m.y.) at ca. 20 Ma was required to reproduce measured AHe and AFT ages, and that the timing and magnitude of this cooling was not sensitive to the timing of burial.

KIRK-1

AHe ages were dispersed in this sample, and no age-eU or age–grain-size correlation was observed. Despite this, AHe ages were reproduced by acceptable fitting paths. These data, plus AFT data, required a modest increase in cooling rate ca. 20 Ma, to rates of ~15 °C/m.y. To allow for the possibility of partial resetting of grains with different pre-depositional histories, hence inherited helium and accumulated radiation damage, we modeled the ZHe single-grain ages separately but simultaneously until deposition at 237–201 Ma. A down side of this independent inheritance approach was that the chance of simulating path sets that simultaneously reproduced ZHe data was extremely low—no good paths were found for 3×10^5 and 7×10^5 simulations. We therefore ran two different models. In one model, we inputted ca. 38 Ma ZHe ages, and in the second, we inputted the ca. 51 Ma ZHe ages.

Inverse modeling results suggested that measured ZHe ages required rapid heating to >200 °C, which is greater than could be reasonably reached with an estimated stratigraphic overburden of ~3 km. We suggest that tectonic burial below the advancing Antalya nappes caused these high temperatures. Modeling results also suggest that ZHe ages record Eocene cooling, which may have been caused by the early formation of the Kirkavak anticline in the late Eocene. An Eocene age of this structure had previously been inferred based on angular discordance between Miocene conglomerates, and underlying Triassic rocks, which record pre-Miocene folding (McPhee et al., 2018a).

BA-1

This sample had dispersed AHe ages. A negative age-eU correlation suggested that additional processes such as helium implantation are required to explain the age dispersion. This prediction was supported by inverse modeling: no time-temperature paths with acceptable or good fits to the data were found during inversion of the data after runs of 10^4 simulations. In Figure 5, we show a model incorporating AFT data only.

PI-01

AFT ages for this sample were older than the age of the Eocene synorogenic rocks sampled, and so we

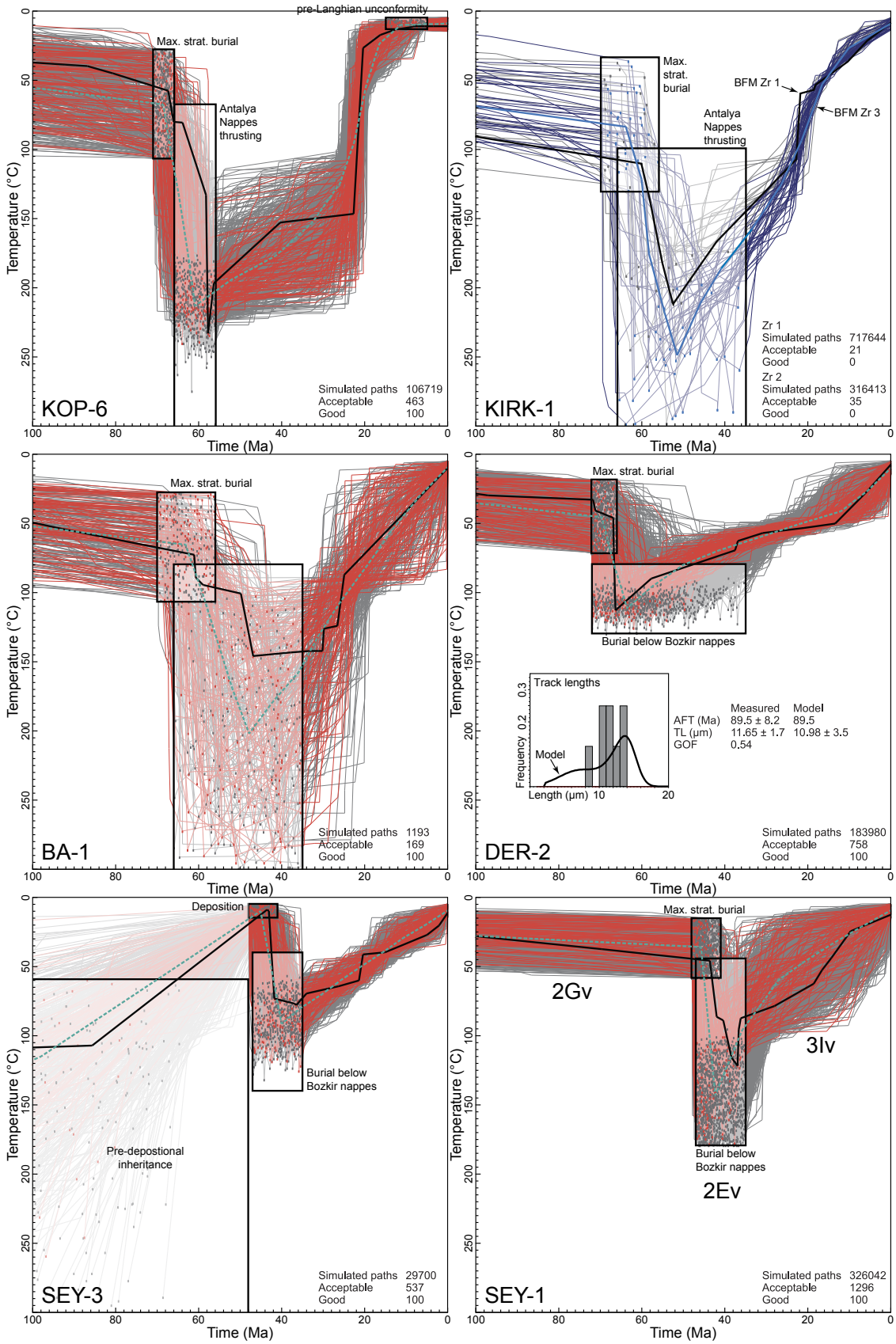

Figure 4. Results of inverse thermal modeling 100 Ma to 0 Ma. Acceptable fitting paths are shown in gray, and good-fitting paths are shown in red. Best-fitting models are thick black lines, and dashed teal line is weighted mean path. All models included pre-depositional *inheritance envelopes* that we cropped out in this figure. Full plots, which include measured and modeled cooling ages, are included in the Supplemental File (text footnote 1). Constraint boxes are described in Table 4 and listed explicitly in the Supplemental File. In KIRK-1, BFM stands for best-fitting model for model runs that incorporated zircon grains 1 and 2, and zircon 3 separately; gray and black paths relate to zircon 1, and blue paths relate to zircons 1 and 2. DER-2 includes measured and predicted track length data.

TABLE 4. PARAMETERS USED IN INVERSE THERMAL MODELING

1. Data treatment	
	AHe data (Table 1)
He ages (Ma)	Raw ages corrected for α-ejection in HeFTy using Ketcham et al. (2011). Individual grains were modelled independently but simultaneously.
Age uncertainty (Ma)	2σ uncertainty applied to raw ages if 2σ ≥ 10%, else 3σ applied.
Rejected data (see also Table 1):	1) SEY-1_3 no grain measurement for α-ejection correction; 2) KOP-6_2,3,4 low eU and Ca; 3) SEY-3_1, KIRK-1_4 outlying ages; 4) SEY-1_1 low eU; 5) DER-2_3 high Th/U and outlying age.
	ZHe data (Table 3)
He ages (Ma)	Raw ages corrected for α-ejection in HeFTy using Ketcham et al. (2011). ZHe ages KIRK-1_3 and KIRK-1_1+2 were run separately (see Fig. 4). ZHe ages SEY-1_1, 2 and 3 were modelled simultaneously, in multi-sample modelling mode.
Age uncertainty (Ma)	2σ uncertainty applied to raw ages if 2σ ≥ 10%, else 3σ applied.
	AFT data (Table 2)
Track length data	Confined track lengths in sample DER-2 only. See Supplemental File (text footnote 1).
Annealing model	Ketcham et al. (2007)
	Vitrinite reflectance (KOP-6 only)
%Ro	Source: Hokerek et al., (2014). Average of 9 measurements from the Upper Triassic Kasımlar Fm. Value used: 2.5 ± 0.34
Uncertainty	2σ standard deviation of 9 published measurements
Calibration	Easy %RO (Sweeny and Burnham, 1990)
2. Geological information	
48–41 Ma	Youngest stratigraphic age Geyikdağı nappe (middle Eocene) (Gutnic et al., 1979)
72–66 Ma	Youngest stratigraphic age Aladağ nappe (Maastrichtian) (Mackintosh and Robertson (2013)
47–35 Ma	Youngest synorogenic rocks involved in thrusting (Gutnic et al., 1979)
66–56 Ma	Age of rocks unconformably covering Antalya-Alanya nappes thrust contacts (Ozgul, 1984)
Stratigraphic overburden	Estimated from Bucak-Seydişehir cross section (McPhee et al., 2018a). See Figure 3.
3. Assumptions	
Surface temperature	10°C ± 5°C
Depositional temperature	10°C ± 5°C
Geothermal gradient	10-40°C/km
Minimum burial temperature	5°C + (10°C x Estimated stratigraphic overburden [km])
Maximum burial temperature	15°C + (40°C x Estimated stratigraphic overburden[km])
4. System and model-specific parameters	
Modelling code:	HeFTy version 1.9.3 (Ketcham et al., 2005)
AHe kinetic model:	RDAAM (Flowers et al., 2009)
ZHe kinetic model:	Guenthner et al. (2013)
AFT Annealing model:	Ketcham et al. (2007)
Statistical fitting criteria:	Good fit = Merit value GOF > 0.5 Acceptable fit = Merit value GOF > 0.05
Number simulated paths:	Inversions run until 100 good-fitting paths found (stopped at >300000 paths for KIRK-1)
t-T path characteristics (Ketcham et al., 2005):	Pre-depositional inheritance = Intermediate monotonic variable (2Iv) Depositional burial heating = Gradual monotonic variable (2Gv) Tectonic burial heating = Episodic monotonic variable (2Ev) Post burial cooling = Intermediate monotonic variable (3Iv)

Notes: AFT—apatite fission-track; AHE—apatite (U-Th)/He; GOF—goodness of fit; ZHe—zircon (U-Th)/He; RDAAM—radiation damage accumulation and annealing; Ro—vitrinite reflectance.

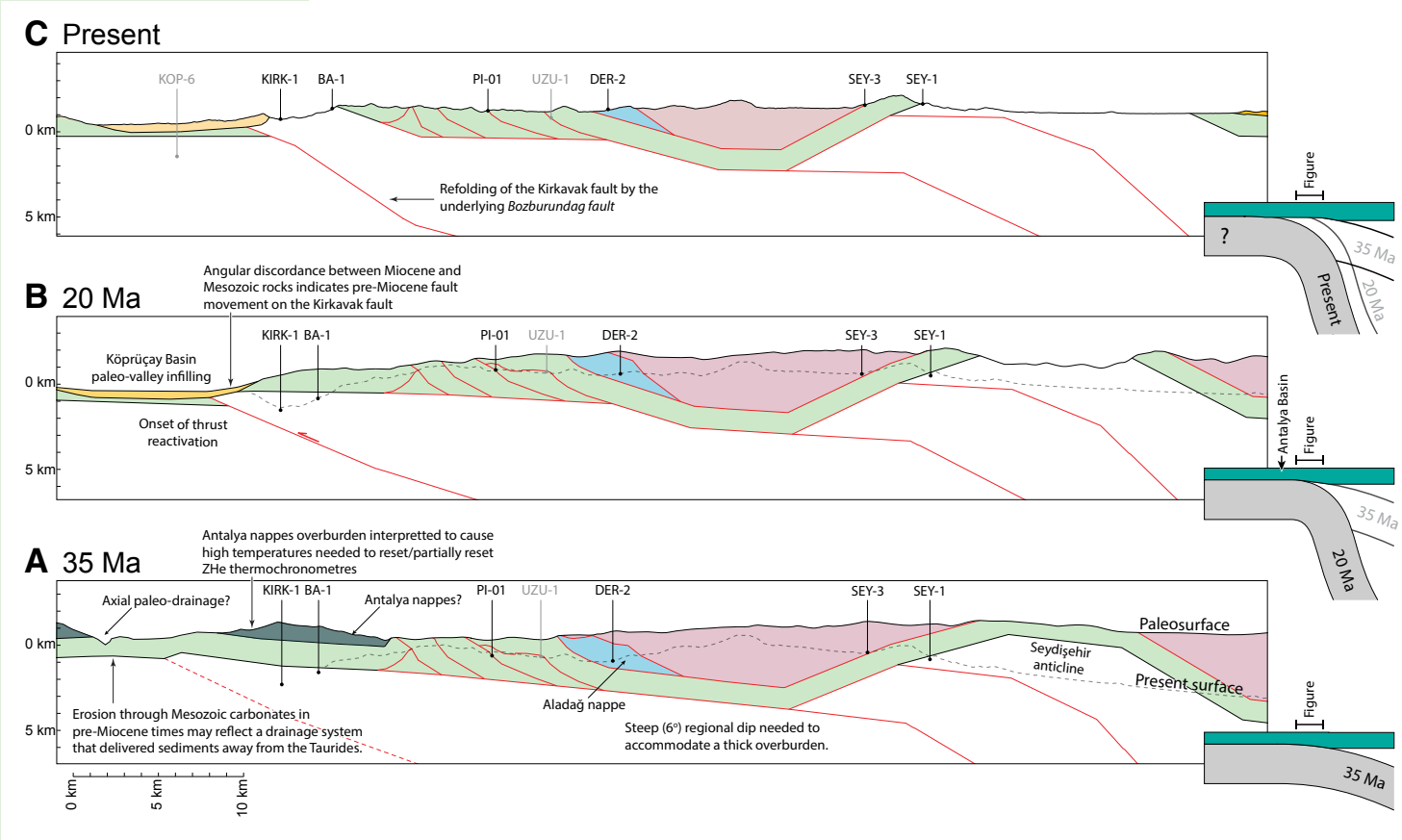

Figure 5. Structural and morphological evolution of the western Central Taurides, along the section line shown in Figures 2 and 3. Small panels show interpreted relationship of the section to the underlying Antalya slab. The interpreted paleosurfaces at 35 Ma and 20 Ma are based on mean temperature from modeling results, a modern average geothermal gradient of ~27 °C/km, and a surface temperature of 10 °C. (A) Late Eocene erosion after thrusting. Widespread Miocene cooling ages in apatite fission-track (AFT) and apatite (U-Th)/He (AHe) thermochronometers suggest that samples remained buried following Eocene thrusting in the belt. Accommodating this overburden requires a regional dip of ~6°. We interpret that the belt was underlain by its original mature and thick mantle lithosphere. (B) Structural interpretation for the early Miocene. Post-early Miocene thrusting and folding are retro-deformed to restore the Köprüçay Basin stratigraphy to horizontal. This phase corresponds to an interpreted increase in cooling rate, which may correspond to uplift and erosion at the onset of delamination. (C) Interpretation of the present-day structure, based on the balanced cross section of McPhee et al. (2018a).

interpreted them as detrital grain ages that represent cooling of the sediment source. This sample was not affected by postdepositional burial and heating sufficient to reset the AFT age. This suggests that the Aladağ and Bozkır nappe systems did not thrust farther than the modern outcrop of the Aladağ nappe.

UZU-1

We interpreted the ca. 21 Ma AFT age as a fully reset age. This early Miocene age may represent the early development of the Üzümdere Valley, which forms part of the modern external drainage system of western Central Taurides.

DER-2

AHe data showed positive age-eU and age–grain-size correlations, suggesting that eU and grain-size variations could account for minor age dispersion. Modeling results suggested that post-Eocene cooling rates with an average of ~1–2 °C/m.y. were needed in this case. We imposed a constraint box from the maximum stratigraphic overburden of 1.4 km in Maastrichtian times (72–66 Ma), based on the youngest stratigraphy in the nappe. The Aladağ nappe was then buried below the Bozkır nappe sometime between Maastrichtian and Eocene times. A mixed AFT age was reproduced in thermal modeling as the product of partial annealing, likely as a result of Late Cretaceous tectonic burial and accretion below the Bozkır nappe. Model results suggest that maximum temperature during this heating pulse was between 90 °C and 130 °C, which reflects the shallow structural position of the Aladağ nappe.

SEY-3

SEY-3 was taken from middle Eocene synorogenic rocks at the top of the Geyikdağı nappe. Reset AHe ages therefore required tectonic burial below the Bozkır and Aladağ nappes. We interpreted an AFT age of ca. 73 Ma as a non-reset or partially reset age. Modeling suggests that this AFT age may be

a result of partial annealing by short-lived heating up to ~130 °C. After burial and heating below the Bozkır and Aladağ nappes, dispersed AHe cooling ages, which were associated with a positive correlation between eU and age and grain size and age were best reproduced by slow rates of cooling (~2 °C/m.y.) after ca. 40 Ma.

SEY-1

An Eocene AFT cooling age from SEY-1 is best explained by localized and structurally controlled erosional exhumation, related to the growth of the Seydişehir anticline. In modeling, we limited the maximum tectonic burial temperature of this sample to 180 °C (using a constraint box), to be consistent with partially reset or inherited AFT ages in the nearby SEY-3 sample. ZHe ages were dispersed. To allow for the possibility of partial resetting of grains with different pre-depositional histories, we modeled the three ZHe ages separately but simultaneously. Dispersed AHe ages could not be reproduced in thermal modeling. Processes such as helium implantation or parent nuclide zonation may have affected the measured grains. We found that by discarding the oldest and youngest AHe ages, the remaining two ca. 10 Ma and ca. 16 Ma AHe ages required slow and constant rates of cooling. We removed the youngest AHe age, because it had a low eU (5 ppm), and we found that remaining AHe data could not be reproduced after runs of $>10^5$ simulations.

6. DISCUSSION

Here we combine our constraints on the thermal evolution of western Central Taurides with structural and stratigraphic constraints to infer morphological evolution, and we link this to the history of uplift and subsidence and to subduction (Fig. 5). We then briefly address the implications for the dynamics of late Miocene plateau rise.

Our results suggest that the Taurides underwent Eocene cooling associated with syn-thrusting, or early post-thrusting erosional exhumation. This cooling was localized to basement-involved thrusts of the Seydişehir anticline and possibly the Kirkavak anticline (Fig. 5A). Elsewhere, there is no positive evidence for significant cooling related to the Eocene phase of thrusting, as well as a lack of volumetrically significant synorogenic sedimentary rocks derived from the Taurides.

A slow post-Eocene to early Miocene cooling rate in samples DER-2 and SEY-1 (supported, but not required, by SEY-3) is highlighted by (1) a large time difference between cooling ages recorded by AFT and AHe thermochronometers; and (2) dispersed AHe ages related to eU and grain-size variations, which in thermal modeling are best reproduced by a long residence time in the AHe partial retention zone due to slow cooling. We interpret this slow cooling as a signal of active, but slow erosional exhumation of a low-elevation, low-relief mountain range. This slowly eroding relative topographic high likely extended to the Manavgat region where Oligocene AFT ages are reported from the structurally higher Alanya nappe by Mittiga (2015).

Fast rates of early to middle Miocene cooling were then recorded in sample KOP-6 and are supported by modeling in sample KIRK-1. This cooling may reflect erosion triggered by the onset of folding and structurally driven rock uplift along the Kirkkavak anticline, during Miocene–Pliocene thrusting in the Antalya Basin (McPhee et al., 2018a) (Fig. 5B). Elsewhere, our model results permit increased early Miocene cooling rates.

Widespread early to middle Miocene cooling ages are time equivalent to the early development of the marine Mut Basin on the southern Central Taurides, defining an along-range variation in rock uplift. In the western Central Taurides, the highest structural units of the Bozkır and Aladağ nappes are preserved as klippen in synclines, and the Geyikdağı nappe has been exhumed from depths of at least a few kilometers, with its Paleozoic or Precambrian basement exposed in the Seydişehir anticline, Köprüçay Valley, and the Hadim area (Fig. 2). In contrast, around the Mut Basin, the Aladağ nappe contains a near complete and continuous stratigraphy and is covered by widespread klippen of the Bozkır nappes, suggesting minimal post-Eocene erosion. We suggest that this along-strike variation in exhumation dominantly reflects early Miocene erosional exhumation. Contrasting post-Eocene structural histories in the western and south Central Taurides can be explained as the result of different dynamic histories of the Antalya and Cyprus slabs (McPhee et al., 2018a). An along-range variation in vertical motion from the western to southern Central Taurides in early to middle Miocene time may then also reflect differing subduction dynamics on the two slabs.

Our reset and partially reset cooling ages require that samples were structurally buried by late Eocene thrusting to at least a few kilometers depth (Fig. 5B). Prior to the Miocene development of the Tauride intramontane basins and the Antalya Basin, any sediment produced by the erosion of the Tauride rocks must have been transported south and south-eastward into the Mediterranean Basin, or toward the backarc region (i.e., the Tuzğolu Basin). The widespread deposition of the Oymapınar limestone in the Antalya Basin in earliest Miocene time demonstrates that there was essentially no siliciclastic sediment production related to the erosion of the Bozkır and Aladağ nappes at that time. From early Miocene to Pliocene times, deposition of the siliciclastic Karpuzçay Formation, which included pebbles derived from the Bozkır nappes (Monod and Kuzucuoğlu, 2019), required an east-to-west–flowing paleodrainage system. This drainage system may be preserved as valleys that cut across the NW-SE structures of the Taurides (Monod et al., 2006). Widespread early Miocene cooling ages, as well as increased rates of cooling recorded in samples KOP-6 and possibly KIRK-1 (plus BA-1), likely record erosional exhumation related to the early development of this Miocene–Pliocene drainage system. Formation of the drainage system may have signaled hinterland uplift (i.e., early uplift in the plateau interior) and the formation of a topographic gradient prior to the development of the modern high-topographic barrier of the Tauride Mountains. Rather than being inherited from Eocene orogenesis, the modern high-topographic barrier thus had an early to middle Miocene origin.

We do not see the effects of the young, ca. 7 Ma and younger surface uplift history of the Central

Anatolian Plateau in our low-temperature thermochronology results, but we may make tentative estimates about the maximum magnitude of late Miocene to present cooling, which must be less than the closure temperature of AHe or AFT systems. In Figures 5B and 5C, we use this magnitude of cooling to estimate erosional exhumation by making some assumptions about the paleogeothermal gradient.

At present, the western Central Tauride crust is estimated to be ~35–40 km thick (Tezel et al., 2013; Vanacore et al., 2013), and given a correlation between crustal thickness and elevation, has been interpreted to be near isostatic equilibrium (McNab et al., 2018; Karabulut et al., 2019), meaning that the crust supports a large part, if not all, of the present elevation of the belt. Palinspastic reconstructions of large-scale Eocene rotations in the Taurides (McPhee et al., 2018b) and evidence from balanced cross sections (McPhee et al., 2018a) show that the present thickness of the crust was assembled by late Eocene time. Despite a ~35–40-km-thick crust, we find that the belt has a volumetrically small synorogenic stratigraphy and experienced low rates of Eocene–Oligocene cooling. We therefore suggest that in Eocene–Oligocene times, the deepest structural unit—the Beydağları platform—was underlying the Tauride fold-thrust belt and was still underlain by its original, mature mantle lithospheric underpinnings that acted as a load on the belt and must have been connected to the Antalya slab.

Seismicity (Kalyoncuoğlu et al., 2011; Howell et al., 2017) and seismic tomography (Biryol et al., 2011; van der Meer et al., 2018) show that the top of the Antalya slab is currently located below the Gulf of Antalya, more than 150 km southwest of Tauride thrusts that mark the Eocene plate boundary. This slab must contain the mantle underpinnings of Taurides, which have now sunk into the mantle. There is no candidate structural expression of slab migration prior to the early Miocene (McPhee et al., 2018a), and so we suggest migration of the slab was achieved by delamination (Fig. 5). Delamination has previously been inferred as a cause of plateau-scale surface uplift (Bartol and Govers, 2014), but here we are instead advocating for delamination on a much smaller scale, recorded by the Eocene to recent vertical motion history of the Central Taurides only.

The Miocene–Pliocene evolution of the western Central Taurides was dominated by extension, thrusting, and oroclinal bending at a highly oblique angle to convergence that was accommodated across the Cyprus slab (Koç et al., 2016; McPhee et al., 2018a) and in contrast to the structurally quiescent development of the Mut Basin (e.g., Cosentino et al., 2012). We suggest that fast rates of Miocene cooling, enigmatic subsidence of the Antalya Basin and subsequent development of a Miocene thrust belt may record the slow and step-wise delamination of the western Central Taurides as follows. Initially, in Eocene–Oligocene time, the Taurides were partly underlain by their original mantle lithospheric underpinnings, connected to the Antalya slab. Next, in Miocene time, slow westward delamination caused subsidence above the slab, forming the Antalya Basin, and caused unloading and uplift localized to the Taurides. The resulting topographic gradient led to gravitational collapse of the Taurides, causing westward-convex oroclinal bending. This oroclinal bending was accommodated by thrusting and modest crustal thickening in the Antalya Basin, which was kinematically balanced by extension and the subsidence in the Central Tauride intramontane basins (Koç et al., 2017). Subsidence in the Antalya Basin may have also driven thin-skinned gravitational sliding of the Lycian nappes over the western edge of Beydağları. The post-late Miocene uplift of marine rocks east of the Köprüçay Basin (Schildgen et al., 2012) was caused by local folding associated with this collapse and is not a regionally important signal of plateau rise. Pliocene uplift of the onshore Antalya Basin, which was associated with the end of thrusting, may record migration of the slab to its current position below the Gulf of Antalya and perhaps full detachment of the slab in the Isparta Angle region to the north. In such a scenario, we predict that much of the modern surface elevation of the western Central Taurides was slowly developed since early to middle Miocene time, independently of processes driving middle to late Miocene uplift of the Mut Basin; these processes occurred above ongoing oceanic subduction and collision with the North African margin.

7. CONCLUSIONS

We present the first thermochronological data from the western Central Taurides in Turkey, and we combine these data with structural and stratigraphic constraints to investigate the history of erosional exhumation in the fold-thrust belt for a time period in which there is no stratigraphic record. Our conclusions are as follows:

(1) Eocene thrusting of the Bozkır and Aladağ nappes over the Geyikdağı platform led to tectonic burial, heating, and resetting of AHe and AFT thermochronometers in many of our samples. Eocene cooling ages recorded localized structurally-driven surface uplift above basement involved structures of the Kirkavak and Seydişehir anticlines.

(2) Early to middle Miocene cooling ages recorded active erosional exhumation at a time of basin formation in the Mut region, suggesting an along-strike change from active subsidence to uplift that we interpret was related to different subduction behavior on the Cyprus and Antalya slabs.

(3) There is no known Eocene–Oligocene stratigraphic record of erosional exhumation that led to Eocene and Oligocene cooling. This suggests that the Mediterranean Basin formed a sediment sink at that time and requires a foreland-dipping paleo-gradient, meaning that the modern topographic barrier of the range formed in early Miocene or later time.

(4) Fast rates of Miocene cooling, the enigmatic development of the Antalya Basin, and subsequent development of a Miocene thrust belt may record the slow and step-wise delamination of the western Central Taurides. We predict that modern surface elevation of the western Central Taurides was slowly developed since early to middle Miocene time.

ACKNOWLEDGMENTS

PJM and DJJvH acknowledge Netherlands Organization for Scientific Research (NWO) Vidi grant 864.11.004 to DJJvH. We are grateful to two anonymous reviewers of an earlier version of this manuscript for their very constructive and helpful comments.

REFERENCES CITED

Akbulut, A., 1977, Etude geologique d'une partie du taurus occidentale au sud d'Egridir (Turquie): Orsay, University Paris-Sud, 203 p.

Altiner, D., Özkan-Altiner, S., and Koçyiğit, A., 2000, Late Permian Foraminiferal Biofacies Belts in Turkey: Palaeogeographic and Tectonic Implications, *in* Bozkurt, E., Winchester, J.A., and Piper, J.D.A., eds., Tectonics and Magmatism in Turkey and the Surrounding Area: Geological Society of London Special Publication 173, no. 1, p. 83–96, https://doi.org/10.1144/GSL.SP.2000.173.01.04.

Andrew, T., and Robertson, A.H.F., 2002, The Beysehir-Hoyran-Hadim Nappes: Genesis and emplacement of Mesozoic marginal and oceanic units of the northern Neotethys in southern Turkey: Journal of the Geological Society of London, v. 159, p. 529–543, https://doi.org/10.1144/0016-764901-157.

Barrier, E., and Vrielynck, B., 2008, Atlas of Paleotectonic Maps of the Middle East (MEBE Program): Commission for the Geological Map of the World, 14 maps (54 × 48 cm) Scale at Equator: 1:18,50,000.

Bartol, J., and Govers, R., 2014, A single cause for uplift of the Central and Eastern Anatolian plateau?: Tectonophysics, v. 637, p. 116–136, https://doi.org/10.1016/j.tecto.2014.10.002.

Biryol, B.C., Beck, S.L., Zandt, G., and Özacar, A., 2011, Segmented African lithosphere beneath the Anatolian region inferred from teleseismic P-wave tomography: Geophysical Journal International, v. 184, p. 1037–1057, https://doi.org/10.1111/j.1365-246X.2010.04910.x.

Ciner, A., Karabiyiko, M., Monod, O., Deynoux, M., and Tuzcu, S., 2008, Late Cenozoic sedimentary evolution of the Antalya Basin, Southern Turkey: Turkish Journal of Earth Sciences, v. 17, July, p. 1–41.

Cosentino, D., Schildgen, T.F., Cipollari, P., Faranda, C., Gliozzi, E., Hudáčková, N., Lucifora, S., and Strecker, M.R., 2012, Late Miocene surface uplift of the southern margin of the Central Anatolian plateau, Central Taurides, Turkey: Geological Society of America Bulletin, v. 124, no. 1, p. 133–145, https://doi.org/10.1130/B30466.1.

Delph, J.R., Abgarmi, B., Ward, K.M., Beck, S.L., Özacar, A.A., Zandt, G., Sandvol, E., and Türkelli, N., 2017, The effects of subduction termination on the continental lithosphere: Linking volcanism, deformation, surface uplift, and slab tearing in central Anatolia: Geosphere, v. 13, no. 6, p. 1788–1805, https://doi.org/10.1130/GES01478.1.

Demirel, I.H., Gunay, Y., and Yurtsever, T.S., 2001, Evaluation of petroleum source rocks on the coastal area of the western Taurus region, Turkey: Energy Sources, v. 23, no. 6, p. 541–552, https://doi.org/10.1080/00908310152125184.

Deynoux, M., Çiner, A., Monod, O., Karabıyıkoglu, M., Manatschal, G., and Tuzcu, S., 2005, Facies architecture and depositional evolution of alluvial fan to fan-delta complexes in the tectonically active Miocene Köprüçay Basin, Isparta Angle, Turkey: Sedimentary Geology, v. 173, no. 1–4, p. 315–343, https://doi.org/10.1016/j.sedgeo.2003.12.013.

Dilek, Y., Thy, P., Hacker, B., and Grundvig, S., 1999, Structure and petrology of Tauride ophiolites and mafic dike intrusions (Turkey): Implications for the Neotethyan Ocean: Geological Society of America Bulletin, v. 111, no. 8, p. 1192–1216, https://doi.org/10.1130/0016-7606(1999)111<1192:SAPOTO>2.3.CO;2.

Dodson, M.H., 1973, Closure temperature in cooling geochronological and petrological systems: Contributions to Mineralogy and Petrology, v. 40, no. 3, p. 259–274, https://doi.org/10.1007/BF00373790.

Farley, K.A., 2000, Helium diffusion from apatite: General behavior as illustrated by Durango fluorapatite: Journal of Geophysical Research. Solid Earth, v. 105, p. 2903–2914, https://doi.org/10.1029/1999JB900348.

Flecker, R., Poisson, A., and Robertson, A.H.F., 2005, Facies and palaeogeographic evidence for the Miocene evolution of the Isparta Angle in its regional eastern Mediterranean context: Sedimentary Geology, v. 173, no. 1–4, p. 277–314, https://doi.org/10.1016/j.sedgeo.2003.10.014.

Flowers, R.M., Ketcham, R.A., Shuster, D.L., and Farley, K.A., 2009, Apatite (U-Th)/He thermochronometry using a radiation damage accumulation and annealing model: Geochimica et Cosmochimica Acta, v. 73, no. 8, p. 2347–2365, https://doi.org/10.1016/j.gca.2009.01.015.

Fernández-Blanco, D., Bertotti, G., Aksu, A., and Hall, J., 2019, Monoclinal flexure of an orogenic plateau margin during subduction, south Turkey: Basin Research, v. 31, p. 709–727, https://doi.org/10.1111/bre.12341.

Galbraith, R.F., and Laslett, G.M., 1993, Statistical models for mixed fission track ages: Nuclear Tracks and Radiation Measurements, v. 21, p. 459–470, https://doi.org/10.1016/1359-0189(93)90185-C.

Glover, C.P., 1995, Plio-Quaternary Sediments and Neotectonics of the Isparta: Edinburgh, Scotland, The University of Edinburgh, 293 p.

Glover, C.P., and Robertson, A.H.F., 1998, Role of regional extension and uplift in the Plio-Pleistocene evolution of the Aksu Basin, SW Turkey: Journal of the Geological Society of London, v. 155, no. 2, p. 365–387, https://doi.org/10.1144/gsjgs.155.2.0365.

Green, P.F., Duddy, I.R., Gleadow, A.J.W., Tingate, P.R., and Laslett, G.M., 1986, Thermal annealing of fission tracks in apatite: 1. A qualitative description: Chemical Geology. Isotope Geoscience Section, v. 59, p. 237–253, https://doi.org/10.1016/0168-9622(86)90074-6.

Guenthner, W.R., Reiners, P.W., Ketcham, R.A., Nasdala, L., and Giester, G., 2013, Helium diffusion in natural zircon: Radiation damage, anisotropy, and the interpretation of zircon (U-Th)/He thermochronology: American Journal of Science, v. 313, no. 3, p. 145–198, https://doi.org/10.2475/03.2013.01.

Guenthner, W.R., Reiners, P.W., and Chowdhury, U., 2016, Isotope dilution analysis of Ca and Zr in apatite and zircon (U-Th)/He chronometry: Geochemistry, Geophysics, Geosystems, v. 17, no. 5, p. 1623–1640, https://doi.org/10.1002/2016GC006311.

Gürer, D., and van Hinsbergen, D.J.J., 2019, Diachronous demise of the Neotethys Ocean as a driver for non-cylindrical orogenesis in Anatolia: Tectonophysics, v. 760, p. 95–106 https://doi.org/10.1016/j.tecto.2018.06.005.

Gürer, D., van Hinsbergen, D.J.J., Özkaptan, M., Creton, I., Koymans, M.R., Cascella, A., and Langereis, C.G., 2018a, Paleomagnetic constraints on the timing and distribution of Cenozoic rotations in Central and Eastern Anatolia: Solid Earth, v. 9, no. 2, p. 295–322, https://doi.org/10.5194/se-9-295-2018.

Gürer, D., Plunder, A., Kirst, F., Corfu, F., Schmid, S.M., and van Hinsbergen, D.J.J., 2018b, A long-lived Late Cretaceous–early Eocene extensional province in Anatolia?: Structural evidence from the Ivriz Detachment, southern central Turkey: Earth and Planetary Science Letters, v. 481, p. 111–124, https://doi.org/10.1016/j.epsl.2017.10.008.

Gutnic, M., Monod, O., Poisson, A., and Dumont, J.-F., 1979, Géologie des Taurides Occidentales (Turquie): Mémoires de la Société Géologique de France, v. 137, p. 1–112.

Hall, J., Aksu, A.E., King, H., Gogacz, A., Yaltırak, C., and Çifçi, G., 2014, Miocene–Recent evolution of the western Antalya Basin and its linkage with the Isparta Angle, eastern Mediterranean: Marine Geology, v. 349, p. 1–23, https://doi.org/10.1016/j.margeo.2013.12.009.

Hokerek, S., Unal, N., Altunsoy, M., Ozcelik, O., and Kuscu, M., 2014, Organic facies characteristics of the Triassic Kasımlar Formation, Anamas-Akseki platform, Western Taurides, Turkey: Energy Procedia, v. 59, p. 150–157, https://doi.org/10.1016/j.egypro.2014.10.361.

Howell, A., Jackson, J., Copley, A., McKenzie, D., and Nissen, E., 2017, Subduction and vertical coastal motions in the eastern Mediterranean: Geophysical Journal International, v. 211, no. 1, p. 593–620, https://doi.org/10.1093/gji/ggx307.

Hurford, A.J., and Green, P.F., 1983, The zeta age calibration of fission-track dating: Chemical Geology, v. 41, p. 285–317, https://doi.org/10.1016/S0009-2541(83)80026-6.

Kalyoncuoğlu, Ü.Y., Elitok, Ö., Dolmaz, M.N., and Anadolu, N.C., 2011, Geophysical and geological imprints of southern Neotethyan subduction between Cyprus and the Isparta Angle, SW Turkey: Journal of Geodynamics, v. 52, no. 1, p. 70–82, https://doi.org/10.1016/j.jog.2010.12.001.

Karabiyikoğlu, M., Ciner, A., Monod, O., Deynoux, M., Tuzcu, S., and Orcen, S., 2000, Tectonosedimentary Evolution of the Miocene Manavgat Basin, Western Taurides, Turkey, *in* Bozkurt, E., Winchester, J.A., and Piper, J.D.A., eds., Tectonics and Magmatism in Turkey and the Surrounding Area: Geological Society of London Special Publication 173, no. 1, p. 271, https://doi.org/10.1144/GSL.SP.2000.173.01.14.

Karabulut, H., Paul, A., Özbakır, A.D., Ergün, T., and Şentürk, S., 2019, A new crustal model of the Anatolia-Aegean domain: Evidence for the dominant role of isostasy in the support of the Anatolian plateau: Geophysical Journal International, v. 218, no. 1, p. 57–73, https://doi.org/10.1093/gji/ggz147.

Ketcham, R.A., 2005, Forward and inverse modeling of low-temperature thermochronometry data: Reviews in Mineralogy and Geochemistry, v. 58, no. 1, p. 275–314, https://doi.org/10.2138/rmg.2005.58.11.

Ketcham, R.A., Donelick, R.A., and Carlson, W.D., 1999, Variability of apatite fission-track annealing kinetics; III, Extrapolation to geological time scales: The American Mineralogist, v. 84, no. 9, p. 1235–1255, https://doi.org/10.2138/am-1999-0903.

Ketcham, R.A., Donelick, R.A., and Carlson, W.D., 2006, Variability of apatite fission-track annealing kinetics: III. Extrapolation to geological time scales (v. 84, p. 1235, 1999): The American Mineralogist, v. 91, no. 2–3, p. 485–486, https://doi.org/10.2138/Am.2006.464.

Ketcham, R.A., Carter, A., Donelick, R.A., Barbarand, J., and Hurford, A.J., 2007, Improved modeling of fission-track annealing in apatite: American Mineralogist, v. 92, p. 799–810, https://doi.org/10.2138/am.2007.2281.

Ketcham, R.A., Gautheron, C., and Tassan-got, L., 2011, Accounting for long alpha-particle stopping distances in (U-Th-Sm)/He geochronology: Refinement of the baseline case: Geochimica et Cosmochimica Acta, v. 75, no. 24, p. 7779–7791, https://doi.org/10.1016/j.gca.2011.10.011.

Koç, A., van Hinsbergen, D.J.J., Kaymakci, N., and Langereis, C.G., 2016, Late Neogene oroclinal bending in the central

Taurides: A record of terminal eastward subduction in southern Turkey?: Earth and Planetary Science Letters, v. 434, no. 1, p. 75–90, https://doi.org/10.1016/j.epsl.2015.11.020.

Koç, A., Kaymakci, N., Van Hinsbergen, D.J.J., and Kuiper, K.F., 2017, Miocene tectonic history of the Central Tauride intramontane basins, and the paleogeographic evolution of the Central Anatolian Plateau: Global and Planetary Change, v. 158, p. 83–102, https://doi.org/10.1016/j.gloplacha.2017.09.001.

Koç, A., van Hinsbergen, D.J.J., and Langereis, C.G., 2018, Rotations of normal fault blocks quantify extension in the Central Tauride Intramontane Basins, SW Turkey: Tectonics, v. 37, no. 8, p. 2307–2327, https://doi.org/10.1029/2018TC005112.

Mackintosh, P.W., and Robertson, A.H.F., 2013, Sedimentary and structural evidence for two-phase Upper Cretaceous and Eocene emplacement of the Tauride thrust sheets in central southern Turkey, *in* Robertson, A.H.F., Parlak, O., and Ünlügenç, U.C., eds., Geological Development of Anatolia and the Easternmost Mediterranean Region: Geological Society [London] Special Publications, v. 372, p. 299–322, https://doi.org/10.1144/SP372.2.

McNab, F., Ball, P.W., Hoggard, M.J., and White, N.J., 2018, Neogene uplift and magmatism of Anatolia: Insights from drainage analysis and basaltic geochemistry: Geochemistry, Geophysics, Geosystems, v. 19, no. 1, p. 175–213, https://doi.org/10.1002/2017GC007251.

McPhee, P.J., and van Hinsbergen, D.J.J., 2019, Tectonic reconstruction of Cyprus reveals Late Miocene continental collision between Africa and Anatolia: Gondwana Research, v. 68, p. 158–173, https://doi.org/10.1016/j.gr.2018.10.015.

McPhee, P.J., Altıner, D., and van Hinsbergen, D.J.J., 2018a, First balanced cross-section across the Taurides fold-thrust belt: Geological constraints on the subduction history of the Antalya slab in southern Anatolia: Tectonics, v. 37, no. 10, p. 3738–3759, https://doi.org/10.1029/2017TC004893.

McPhee, P.J., van Hinsbergen, D.J.J., Maffione, M., and Altiner, D., 2018b, Palinspastic reconstruction versus cross-section balancing: How complete is the Central Taurides fold-thrust belt (Turkey)?: Tectonics, v. 37, p. 4285–4310, https://doi.org/10.1029/2018TC005152.

Meesters, A.G.C., and Dunai, T., 2002, Solving the production-diffusion equation for finite diffusion domains of various shapes: Chemical Geology, v. 186, no. 3–4, p. 333–344, https://doi.org/10.1016/S0009-2541(01)00422-3.

Meijers, M.J.M., Brocard, G.Y., Cosca, M.A., Lüdecke, T., Teyssier, C., Whitney, D.L., and Mulch, A., 2018, Rapid late Miocene surface uplift of the Central Anatolian Plateau margin: Earth and Planetary Science Letters, v. 497, p. 29–41, https://doi.org/10.1016/j.epsl.2018.05.040.

Mittiga, F., 2015, Low-temperature thermochronological evolution of the Menderes and Alanya massifs [Ph.D. thesis]: Università di Bologna, 207 p.

Monod, O., and Kuzucuoğlu, C., 2019, A Fossil Morphology: The Miocene Fluvial Network of the Western Taurus (Turkey), *in* Kuzucuoğlu, C., Çiner, A., and Kazancı, N., eds., Landscapes and Landforms of Turkey: Cham, Switzerland, Springer International Publishing, p. 385–395, https://doi.org/10.1007/978-3-030-03515-0_19.

Monod, O., Kuzucuoğlu, C., and Okay, A.I., 2006, A Miocene palaeovalley network in the western Taurus (Turkey): Turkish Journal of Earth Sciences, v. 15, p. 1–23.

Öğretmen, N., Cipollari, P., Frezza, V., Faranda, C., Karanika, K., Gliozzi, E., Radeff, G., and Cosentino, D., 2018, Evidence for 1.5 km of uplift of the Central Anatolian Plateau's southern margin in the last 450 kyr and implications for its multiphased uplift history: Tectonics, v. 37, p. 359–390, https://doi.org/10.1002/2017TC004805.

Özgül, N., 1976, Some geological aspects of the Taurus orogenic belt (Turkey): Bulletin of the Geological Society of Turkey, v. 19, p. 65–78 (in Turkish with English abstract).

Özgül, N., 1984, Stratigraphy and tectonic evolution of the central Taurus: Proceedings of International Symposium on the Geology of the Taurus Belt, 1983, General Directorate of Mineral Research and Exploration (MTA), p. 77–90.

Peyton, S.L., and Carrapa, B., 2013, An introduction to low-temperature thermochronologic techniques, methodology, and applications, *in* Knight, C.N., Cuzella, J.J., and Cress, L.D., eds., Application of Structural Methods to Rocky Mountain Hydrocarbon Exploration and Development: American Association of Petroleum Geologists, Studies in Geology, v. 65, p. 15–36, https://doi.org/10.1306/13381688St653578.

Poisson, A., Akay, E., Cravatte, J., Muller, C., and Uysal, S., 1983, Donnees nouvelles sur la chronologie de mise en place des nappes d'Antalya au centre de l'angle d'Isparta (Taurides occidentales, Turquie): Comptes Rendus des Seances, Academie des Sciences, Serie II., v. 296, p. 923–925.

Poisson, A., Roland, W., Sağular, K., and Temiz, H., 2003, New data concerning the age of the Aksu Thrust in the south of the Aksu valley, Isparta Angle (SW Turkey): Consequences for the Antalya Basin and the Eastern Mediterranean: Geological Journal, v. 38, p. 311–327, https://doi.org/10.1002/gj.958.

Poisson, A., Orszag-Sperber, F., Kosun, E., Bassetti, M.A., Muller, C., Wernli, R., and Rouchy, J.M., 2011, The late Cenozoic evolution of the Aksu basin (Isparta Angle; SW Turkey): New insights: Bulletin de la Société Géologique de France, v. 182, no. 2, p. 133–148, https://doi.org/10.2113/gssgfbull.182.2.133.

Portner, D.E., Delph, J.R., Biryol, C.B., Beck, S.L., Zandt, G., Özacar, A.A., Sandvol, E., and Türkelli, N., 2018, Subduction termination through progressive slab deformation across Eastern Mediterranean subduction zones from updated P-wave tomography beneath Anatolia: Geosphere, v. 14, no. 3, p. 907–925, https://doi.org/10.1130/GES01617.1.

Pourteau, A., Candan, O., and Oberhänsli, R., 2010, High-pressure metasediments in central Turkey: Constraints on the Neotethyan closure history: Tectonics, v. 29, no. 5, TC5004, https://doi.org/10.1029/2009TC002650.

Reiners, P.W., and Brandon, M.T., 2006, Using thermochronology to understand orogenic erosion: Annual Review of Earth and Planetary Sciences, v. 34, no. 1, p. 419–466, https://doi.org/10.1146/annurev.earth.34.031405.125202.

Reiners, P.W., Spell, T.L., Nicolescu, S., and Zanetti, K.A., 2004, Zircon (U-Th)/He thermochronometry: He diffusion and comparisons with $^{40}Ar/^{39}Ar$ dating: Geochimica et Cosmochimica Acta, v. 68, no. 8, p. 1857–1887, https://doi.org/10.1016/j.gca.2003.10.021.

Robertson, A.H.F., 2004, Development of concepts concerning the genesis and emplacement of Tethyan ophiolites in the Eastern Mediterranean and Oman regions: Earth-Science Reviews, v. 66, no. 3–4, p. 331–387, https://doi.org/10.1016/j.earscirev.2004.01.005.

Royden, L., and Faccenna, C., 2018, Subduction orogeny and the late Cenozoic evolution of the Mediterranean arcs: Annual Review of Earth and Planetary Sciences, v. 46, no. 1, p. 261–289, https://doi.org/10.1146/annurev-earth-060115-012419.

Schildgen, T.F., Cosentino, D., Caruso, A., Buchwaldt, R., Yıldırım, C., Bowring, S.A., Rojay, B., Echtler, H., and Strecker, M.R., 2012, Surface expression of eastern Mediterranean slab dynamics: Neogene topographic and structural evolution of the southwest margin of the Central Anatolian Plateau, Turkey: Tectonics, v. 31, https://doi.org/10.1029/2011TC003021.

Schildgen, T.F., Yıldırım, C., Cosentino, D., and Strecker, M.R., 2014, Linking slab break-off, Hellenic trench retreat, and uplift of the Central and Eastern Anatolian plateaus: Earth-Science Reviews, v. 128, p. 147–168, https://doi.org/10.1016/j.earscirev.2013.11.006.

Şengör, A.M., and Yilmaz, Y., 1981, Tethyan evolution of Turkey: A plate tectonic approach: Tectonophysics, v. 75, no. 3–4, p. 181–241, https://doi.org/10.1016/0040-1951(81)90275-4.

Seyitoğlu, G., Işik, V., Gürbüz, E., and Gürbüz, A., 2017, The discovery of a low-angle normal fault in the Taurus Mountains: The İvriz detachment and implications concerning the Cenozoic geology of southern Turkey: Turkish Journal of Earth Sciences, v. 26, p. 189–205.

Shuster, D.L., and Farley, K.A., 2009, The influence of artificial radiation damage and thermal annealing on helium diffusion kinetics in apatite: Geochimica et Cosmochimica Acta, v. 73, no. 1, p. 183–196, https://doi.org/10.1016/j.gca.2008.10.013.

Shuster, D.L., Flowers, R.M., and Farley, K.A., 2006, The influence of natural radiation damage on helium diffusion kinetics in apatite: Earth and Planetary Science Letters, v. 249, no. 3–4, p. 148–161, https://doi.org/10.1016/j.epsl.2006.07.028.

Sweeney, J.J., and Burnham, A.K., 1990, Evaluation of a simple model of vitrinite reflectance based on chemical kinetics: American Association of Petroleum Geologists Bulletin, v. 74, p. 1559–1570, https://doi.org/10.1306/0C9B251F-1710-11D7-8645000102C1865D.

Tezel, T., Shibutani, T., and Kaypak, B., 2013, Crustal thickness of Turkey determined by receiver function: Journal of Asian Earth Sciences, v. 75, p. 36–45, https://doi.org/10.1016/j.jseaes.2013.06.016.

Vanacore, E.A., Taymaz, T., and Saygin, E., 2013, Moho structure of the Anatolian plate from receiver function analysis: Geophysical Journal International, v. 193, no. 1, p. 329–337, https://doi.org/10.1093/gji/ggs107.

van der Meer, D.G., van Hinsbergen, D.J.J., and Spakman, W., 2018, Atlas of the underworld: Slab remnants in the mantle, their sinking history, and a new outlook on lower mantle viscosity: Tectonophysics, v. 723, p. 309–448, https://doi.org/10.1016/j.tecto.2017.10.004.

van Hinsbergen, D.J.J., Kaymakci, N., Spakman, W., and Torsvik, T.H., 2010, Reconciling the geological history of western Turkey with plate circuits and mantle tomography: Earth and Planetary Science Letters, v. 297, no. 3–4, p. 674–686, https://doi.org/10.1016/j.epsl.2010.07.024.

van Hinsbergen, D.J.J., Maffione, M., Plunder, A., Kaymakcı, N., Ganerød, M., Hendriks, B.W.H., Corfu, F., Gürer, D., de Gelder, G.I.N.O., Peters, K., McPhee, P.J., Brouwer, F.M., Advokaat, E.L., and Vissers, R.L.M., 2016, Tectonic evolution and paleogeography of the Kırşehir Block and the Central Anatolian Ophiolites, Turkey: Tectonics, v. 35, no. 4, p. 983–1014, https://doi.org/10.1002/2015TC004018.

Vermeesch, P., and Tian, Y., 2014, Thermal history modelling: HeFTy vs. QTQt: Earth-Science Reviews, v. 139, p. 279–290, https://doi.org/10.1016/j.earscirev.2014.09.010.